Biochemistry

 Volume 40, Number 33 August 21, 2001

Accelerated Publications

Probing Inhibitors Binding to Human Urokinase Crystals by Raman Microscopy: Implications for Compound Screening†

Jian Dong,‡ Kerry Swift,§ Edmund Matayoshi,§ Vicki L. Nienaber,§ Moshe Weitzberg,§ Todd Rockway,§ and Paul R. Carey*,‡

Department of Biochemistry, School of Medicine, Case Western Reserve University, 10900 Euclid Avenue, Cleveland, Ohio 44106-4935, and Department of Structural Biology, Abbott Laboratories, 100 Abbott Park Road, D-46Y, Building AP9, Abbott Park, Illinois 60064-6114

Received May 10, 2001; Revised Manuscript Received July 5, 2001

ABSTRACT: Inhibition of urokinase activity represents a promising target for antimetastatic therapy for several types of tumor. The present study sets out to investigate the potential of Raman spectroscopy for defining the molecular details of inhibitor binding to this enzyme, with emphasis on single crystal studies. It is demonstrated that high quality Raman spectra from a series of five inhibitors bound individually to the active site of human urokinase can be obtained in situ from urokinase single crystals in hanging drops by using a Raman microscope. After recording the spectrum of the free crystal, a solution of inhibitor containing an amidine functional group on a naphthalene ring was added, and the spectrum of the crystal−inhibitor complex was obtained. The resulting difference Raman spectrum contained only vibrational modes due to bound inhibitor, originating from the protonated group, i.e., the amidinium moiety, as well as naphthalene ring modes and features from other functionalities that made up each inhibitor. The identification of the amidinium modes was placed on a quantitative basis by experimental and theoretical work on naphthamidine compounds. For the protonated group, $-C-(NH_2)_2^+$, the symmetric stretch occurs near 1520 cm^{-1}, and a less intense antisymmetric mode appears in the Raman spectra near 1680 cm^{-1}. The presence of vibrational modes near 1520 cm^{-1} in each of the Raman difference spectra of the five complexes examined unambiguously identifies the protonated form of the amidinium group in the active site. Several advantages were found for single crystal experiments over solution studies of inhibitor−enzyme complexes, and these are discussed. The use of single crystals permits competitive binding experiments that cannot be undertaken in solution in any kind of homogeneous assay format. The Raman difference spectrum for a single crystal that had been exposed to equimolar amounts of all five inhibitors in the hanging drop showed only the Raman signature of the compound with the lowest K_i . These findings suggest that the Raman approach may offer a route in the screening of compounds in drug design applications as well as an adjunct to crystallographic analysis.

Structure-based drug design has become a powerful means of identifying and refining novel pharmaceutical compounds. The two principal techniques used to define the structures of protein−drug complexes are X-ray crystallography and NMR,[1] and in both cases computer-based modeling is used to consolidate and extend the experimental data. Other

† This work was supported by NIH Grant GM-54072 (to P.R.C.).

* Correspondence should be addressed to this author at the Department of Biochemistry, School of Medicine, Case Western Reserve University, Cleveland, OH 44106-4935. Phone: (216)368-0031. FAX: (216)368-3419. E-mail: carey@biochemistry.cwru.edu.

‡ Case Western Reserve University.

§ Abbott Laboratories.

[1] Abbreviations: UK, urokinase; MW, molecular weight; K_i, inhibition constant; S2444, H-D-pyroglutamyl-Gly-L-Arg-*p*-nitroanilide; Tris, tris(hydroxymethyl)aminomethane; DMSO, dimethyl sulfoxide; CCD, charge-coupled device; mW, milliwatt(s); DFT, density functional theory; NMR, nuclear magnetic resonance.

10.1021/bi010955+ CCC: $20.00
Published on Web 07/26/2001

Scheme 1: Urokinase Inhibitors: Structure and Inhibition Constant

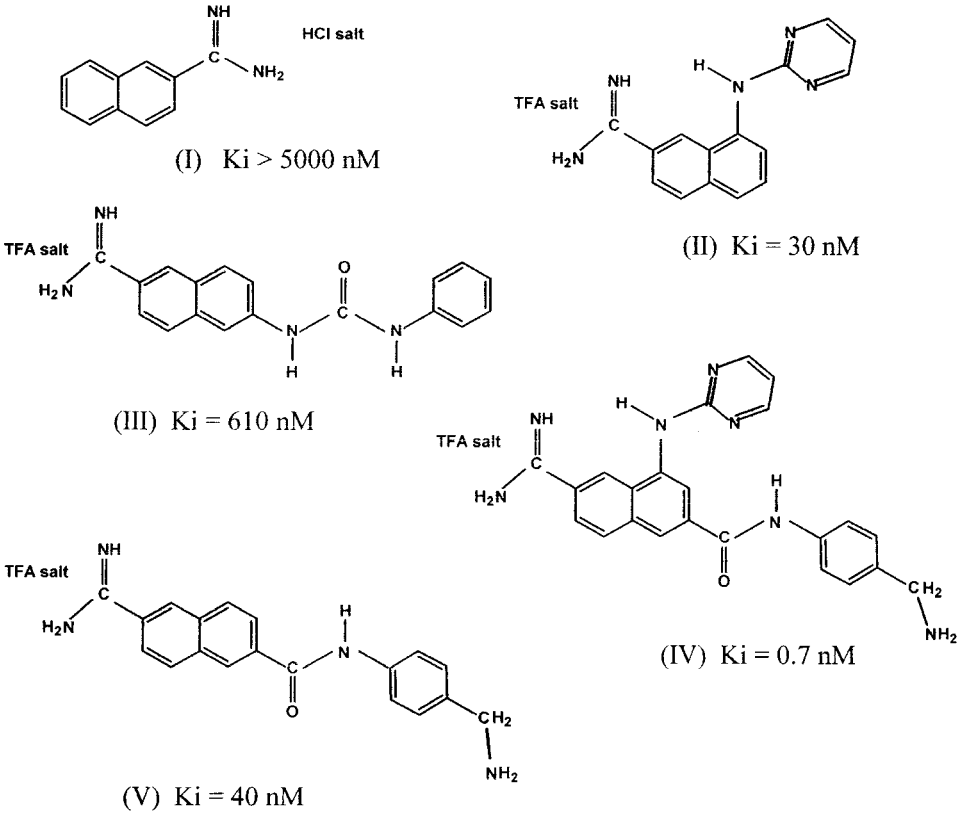

biophysical techniques may be of value in pursuing these goals; for example, we have shown recently that Raman spectroscopy is capable of probing protein−ligand interactions in single crystals as well as in solution and can thus bridge the gap between studies undertaken in the two phases (*1*). The information content from Raman data is more limited compared to that from X-ray or NMR, but while the latter techniques can provide overall structural information, Raman can complement this and fill in details that are lacking from the more global techniques. For example, Raman spectroscopy can often identify a group's protonation state—information that is nearly always lacking from crystallographic analysis. Our initial study demonstrated that, by using Raman difference spectroscopy, different conformational states could be identified for the flavin cofactor bound to the enzyme *p*-hydroxybenzoate hydroxylase (PHBH). Moreover, these states could be compared for complexes in solution and in single crystals (*1*). The Raman spectra from the crystals were obtained in situ in hanging drops. The flavin is an endogenous ligand for PHBH, and we now show that the approach is equally amenable to the study of exogenous ligands. The system selected to demonstrate the principles involves the enzyme urokinase (UK) and a series of compounds that were developed in the search for an inhibitor for urokinase that would be of therapeutic value.

Human urokinase is a trypsin-like serine protease of molecular mass 47.7 kDa with 424 amino acids. It has been shown to be strongly associated with tumor cells (*2*) and to play a role in basement membrane degradation with the concomitant activation of plasminogen and metalloproteases (*3*−*6*). Furthermore, inhibitors of urokinase have been reported to slow tumor metastasis as well as growth of the primary tumor (*7*−*15*). Thus, urokinase has been a target for potent inhibitors that could be of value in cancer therapy. In the present instance, a series of inhibitors was developed based on naphthamidine as the parent compound, and five members of the series are shown in Scheme 1. The K_i values for compounds I−V vary over approximately 5000-fold with the best inhibitor, compound IV, having a K_i in the subnanomolar range. Recently, crystals of a re-engineered UK, MW = 28 000, consisting of residues Ile159−Lys404 in the catalytic B-chain with the two mutations C279A and N302Q, have been obtained in a form that permits facile inhibitor soaking into single crystals (*16*). Here, we demonstrate that Raman spectra can be obtained for compounds I−V bound individually to crystals of micro-urokinase and that the data are superior to those obtained for the same complexes in solution. The data provide unequivocal evidence that the amidine group on each inhibitor binds in the protonated amidinium form. Moreover, in a competitive inhibition, screening-type, Raman experiment on a single crystal in a hanging drop, it was possible to identify the inhibitor with the lowest K_i.

EXPERIMENTAL PROCEDURES

Materials. Stock solutions of the compounds were prepared at 2−20 mM in DMSO. For competitive binding studies, a mixture of the five compounds was prepared at equimolar concentrations of 4 mM in DMSO. The UK used in this study, a re-engineered form, consisting of residues Ile159−Lys404 in the B-chain with the two mutations C279A and N302Q, was prepared by polymerase chain reaction manipulations as described previously by Nienaber et al. (*16*). The inhibitory effect of the compounds on the steady-state amidolytic activity of UK was characterized by

using a chromogenic substrate, S2444, as previously described (*16, 17*).

Crystals of UK were grown by the vapor diffusion method as described in Nienaber et al. (*16*). Briefly, the well solution contained 0.15 M succinate buffer, pH 4.7, 20% poly(ethylene glycol) (MW = 4000), and 0.15 M Li_2SO_4. The hanging drops contained 2 μL of the well solution and 2 μL of the protein solution. The crystals were grown to an approximate dimension of 100 μm × 30 μm × 30 μm.

Preparation of Crystal Complexes. Two diffusion approaches were used to obtain the crystals of UK complexes: (1) In situ soaking: 0.5−1.0 μL of DMSO solution of the amidine ligand (5 mM) was added to a hanging drop (~3 μL) containing a native crystal, the hanging drop was allowed to incubate for about 1 h before the drop solution became a transparent single phase, and a Raman spectrum was recorded for the crystal under the glass coverslip without removing the DMSO and excess ligand. For a crystal of linear dimensions 100 μm × 50 μm × 50 μm with a protein concentration of 27 mM [estimated according to the unit cell dimensions of UK (*16*)], the number of active sites in the crystal is only 0.7% of the number of ligand molecules contained in 1 μL of a 1 mM solution. Therefore, if the dissociation constant is at the micromolar level or less, the ligand can concentrate within the crystal to an almost 27 mM level, even though its concentration in the surrounding medium and in the solvent channels of the crystal remains close to 1 mM. (2) Ex situ soaking: The native protein crystals were transferred to the mother liquor (10−50 μL), to which 1.0 μL of a 10−20 mM compound solution in DMSO had been added. The crystals were allowed to incubate for 24 h at 18 °C and transferred under the microscope into a fresh hanging drop (3 μL) of the crystallization mother liquor and equilibrated for at least 1 h to remove DMSO and any compound bound nonspecifically. For compounds I and V, only the in situ soaking was performed; however, for the other three compounds and for the mixture of all five, ex situ soaking gave slightly better results.

Raman Spectroscopy. The protein crystals in the hanging drops (i.e., under growth conditions) were placed in the focused laser beam with the help of a Raman microscope system (configured with an Olympus BH 60 microscope), as described by Altose et al. (*1*). Then 50 mW of 647.1 nm laser excitation from a krypton laser (Coherent Innova 400 laser system) was delivered along the optical axis of the microscope to generate the off-resonance Raman scattering under a 50× objective, with backscattering geometry. Real-time color video display with direct viewing of the laser focal point ensured that no photochemical damage occurred to the crystals. An optical fiber transfers Raman photons from the microscope to the fore-optics of a high-throughput f/1.4 axial transmissive spectrograph (Kaiser Optical Systems, Inc.) (*18*). Using an entrance slit of 50 μm, the spectrograph displays neon-lamp line widths of approximately 5.9 cm^{-1} (fwhm) at the Raman shift region of 1235 cm^{-1} for a 1024 pixel-wide charge-coupled device (CCD) detector (operated at a temperature of 183 K, from Princeton Instruments, Inc.). Raman spectra of native and bound crystals and buffer were collected by binning 40 horizontal rows of CCD pixels. Before performing the subtraction of the Raman spectra [UK crystal + ligand] − [UK crystal], buffer and solvent spectra were subtracted according to the following protocol. A spectrum of a native crystal was acquired for 5 min CCD exposure time, and is denoted as spectrum A; then a spectrum of the mother liquor was recorded after translating the hanging drop by approximately 50 μm so that the laser focal point is shifted away from the crystal, giving spectrum B. A Raman difference spectrum, C, of native protein in the crystal is derived by computer subtraction: spectrum C = spectrum A − spectrum B. This process removes the Raman bands due to the buffer and crystallization media that are present in the crystal channels. Subsequently, a Raman spectrum of the crystal with a ligand bound was recorded over the same CCD exposure time, denoted as spectrum D, which also contains an appreciable amount of solvent signals. A spectrum of the mother liquor (which contains organic solvent used as a carrier in the in situ soaking method) was recorded after shifting the laser focal point by approximately 50 μm away from the complex crystal, generating spectrum E; and a Raman difference spectrum of the protein complex in the crystalline state, spectrum F, was acquired by computer subtraction: spectrum F = spectrum D − spectrum E. Finally, a Raman spectrum of the ligand bound in the protein crystal, spectrum G, was obtained by the subtraction method: spectrum G = spectrum F − spectrum C. In the subtraction procedures, a scaling factor was used to reduce the contribution of buffer peaks to zero. The success of this procedure is demonstrated by the absence of mother liquor bands in spectrum G (seen for all five ligands in Figure 2), except for those of the intense sulfate band at 980 cm^{-1}.

In solution studies, Raman spectra were obtained using 752 nm laser excitation from the same laser system under the 90° excitation/collection geometry. A slit width of 250 μm was set in the spectrograph, and 60 horizontal rows of CCD were binned. Protein samples at ~170 μM (50 μL) buffered with 50 mM Tris-HCl at pH 7.5 were held in a 2 × 2 mm ID glass cuvette. After obtaining the Raman spectrum of the protein, the ligand in aqueous or DMSO solution was added in a quantity equal to the concentration of protein, and the data were collected immediately after the complex had been made, using a laser power of 850−950 mW with a CCD exposure time of 5 min. The Raman spectrum of the buffer (or DMSO solvent) was subtracted from that of the ligand in buffer (or DMSO solvent) to give the spectrum of free ligand. The spectrum of the protein in buffer was subtracted from that of the protein−ligand complex in buffer to give the spectrum of the protein-bound ligand. The subtraction of data sets was performed using GRAMS/32 software (Galactic Industries, Inc.).

Quantum mechanical computations have been performed to analyze the vibrational assignments of compounds I, II, and III (Scheme 1), using Gaussian 98 software (*19*). In addition, benzamidinium cationic and neutral forms, 2-aminopyrimidine, carbanilide (*N*,*N*′-diphenylurea), and benzanilide (*N*-phenylbenzamide), were also analyzed to confirm the amidinium/amidine vibrational modes, the ring modes of the pyrimidine, the ureido group, and the aromatic amide group vibrational modes, respectively. The calculations provide a priori knowledge of the Raman spectrum of an entire molecule or a part of the functional group(s) for identification. Full geometry optimization of the molecules was carried out for the subsequent estimation of harmonic force constants at the same density functional theory (DFT) level (Becke's three-parameter hybrid functional using the

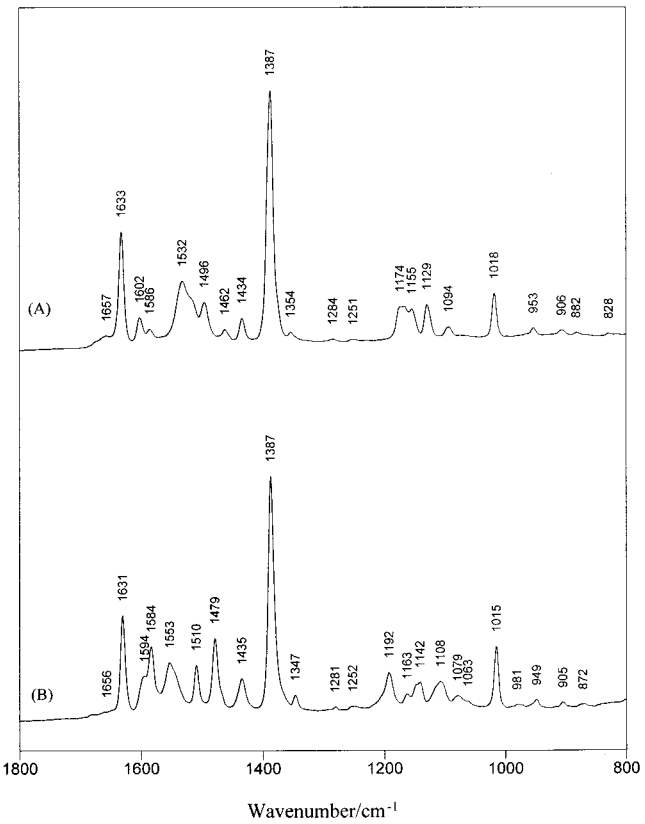

FIGURE 1: Raman spectra of 50 mM 2-naphthamidine at pH 1 (A) and pH 13 (B). 647.1 nm laser excitation, 50 mW backscattering geometry under microscope 10× objective, 5 min data accumulation.

correlation functional of Lee, Yang, and Parr, B3LYP). Gaussian basis sets of 6-31+G(d), 6-31G*, 6-31G, 6-31+G(d,p), 6-31+G(d,p), 6-31+G(d), and 6-31+G(d) were used for compound I (at cationic and neutral states), II (at cationic state only), III (at cationic state only), benzamidine (at cationic and neutral states), 2-aminopyrimidine, carbanilide, and benzanilide, respectively. The absence of imaginary wavenumbers confirmed that the optimized geometries correspond well to the ground state energy minima. The raw frequencies were converted by a single scaling factor of 0.985 through a least-squares approach, mainly to correct for the anharmonicity, according to the work of Scott and Radom (*20*). Only the DFT frequencies of the 2-naphthamidine cation are listed here.

RESULTS AND DISCUSSION

Assignment of the Naphthyl Ring and Amidinium Modes of 2-Naphthamidine. 2-Naphthamidine (compound I in Scheme 1) has been pursued vigorously as a lead scaffold in the search for potent compounds that exhibit selectivity against urokinase-tissue plasminogen activator. It is the parent compound for the five inhibitors studied here and depicted in Scheme 1. Thus, an understanding of the normal modes of 2-naphthamidine provides the starting point for interpretation of the Raman spectra of compounds I−V (Scheme 1). The Raman spectra of I at pH 1 (amidinium, protonated) and pH 13 (amidine, neutral) are compared in Figure 1. Density functional theory calculations, at the B3LYP/6-31+G(d) level, provide a detailed interpretation of the Raman spectra. The results of the calculations are given in Table 1 , and the agreement between experiment and theoretical band positions is good, usually ±6 cm^{-1}. The most intense Raman modes are due to naphthyl ring vibrations with features near 1630 and 1390 cm^{-1} and between 1160 and 1190 cm^{-1} being highly characteristic (*21*).

Key marker bands concern the amidinium moiety. For the protonated form, a weak band near 1670 cm^{-1} [Table 1 and spectrum A in the supplemental figure (see Supporting Information), seen as a weak shoulder in Figure 1A] arises from a vibrational mode due to antisymmetric N−C−N

Table 1: Summary of Major Raman Bands of Naphthamidinium (Frequencies in cm^{-1})[a]

observed	calculated	assignments
1671w	1677.6	two NH_2 groups anti-phase scissoring + N−C−N antisymmetric stretching
1663w	1669.2	two NH_2 groups in-phase scissoring
1633s	1632.5	ring stretching
1601w	1607.6	ring stretching
1588w	1581.2	ring stretching + NH_2 scissoring
1540m	1542.1	N−C−N antisymmetric stretching + NH_2 anti-phase scissoring
1525s	1517.1	N−C−N symmetric stretching + ring stretching + NH_2 scissoring
1499m	1503.4	$C_2-C_{(a)}$ stretching + N−C−N symmetric stretching + NH_2 scissoring + ring stretching
1471w	1465.0	ring stretching + $C_2-C_{(a)}$ stretching + NH_2 scissoring
1436w	1448.8	ring stretching
1392s	1398.2	ring I Kekulé stretching
1380s	1386.7	ring II Kekulé stretching
1356w	1362.2	ring stretching
1284w	1279.6	ring stretching
1260w	1258.5	ring stretching
1229w	1223.0	ring stretching
1183w	1174.1	ring II C−H in-plane bending
1164m	1171.6	ring I C−H + ring II C−H in-plane bending
1152w	1155.9	ring I C−H + ring II C−H + $C_{(a)}-C_2$ stretching + N−C bending
1128m	1124.5	ring C−H + $C_{(a)}-C_2$ stretching + NH_2 bending
1087w	1079.5	N−C−N in-plane bending + two NH_2 symmetric bending
	1049.6	two NH_2 group asymmetric bending
1020s	1027.1	ring I in-plane bending
	1001.3	ring I C−H out-of-plane bending
975w	972.7	ring I and ring II C−H out-of-plane bending
	960.7	ring I and ring II C−H out-of-plane bending
951w	945.0	ring I and ring II C−H in-plane bending
912w	904.1	ring I and ring II C−H out-of-plane bending
882w	876.0	two ring in-plane bending
	870.1	ring C−H out-of-plane bending
	814.6	ring C−H out-of-plane bending
780s	765.4	two ring breathing
766sh	756.2	C−H out-of-plane bending
	751.4	$C_2-C_{(a)}$ out-of-plane bending
701w	707.0	ring in-plane bending + N−C−N in-plane bending

[a] Observed frequencies for solid naphthamidinium cation $[(C_{11}H_{11}N_2)^+Cl^-]$ are shown in the supplementary figure, spectrum (A) (see Supporting Information).

stretching coupled to NH_2 deformation, while the broad complex band ranging from 1540 to 1500 cm^{-1} (Figure 1A) is made up of three different normal modes with close vibrational energies—containing either N−C−N antisymmetric stretching or symmetric stretching character—with various degrees of coupling to NH_2 deformation and naphthalene ring stretching. The band due to the antisymmetric stretching component is located in the region from 1560 to 1540 cm^{-1} and has lower Raman intensity, whereas the band due to the symmetric stretching component is located from 1540 to 1520 cm^{-1} with higher intensity. These assignments have been confirmed by normal mode analyses of other ligands (compounds II and III in Scheme 1, and the benzamidinium cation), all of which have produced quite similar normal mode structures for the amidinium group (unpublished data). Further confirmation is found in the fact that the Raman spectrum of each compound, I−V, shows a similar medium intensity profile in the 1500−1540 cm^{-1} region (see Supporting Information). Moreover, replacing the 2-amidinium group in compound II (Scheme 1) by a 2-cyano group results in the disappearance of this marker band, but without altering the spectral pattern of the naphthalene ring mode (unpublished work, this laboratory).

For the neutral form of the amidine group at pH 13, Figure 1B shows that the medium intensity band of the amidinium group near 1530 cm^{-1} (in Figure 1A) disappears. A new suite of bands between 1479 and 1631 cm^{-1} in Figure 1B is due to naphthyl ring modes that are coupled to the C═N stretching mode. A mode that is predominantly C═N stretch appears as a weak and poorly defined feature ranging from 1640 to 1660 cm^{-1}, barely discernible in Figure 1B, and is assigned based on our density functional analysis. Likewise, the Raman spectrum of benzamidine (data not shown here) shows that the marker bands for the benzamidinium cation at 1528 cm^{-1} (medium intensity) and 1676 cm^{-1} (weak intensity) disappear upon deprotonation at pH 13, whereas new bands at 1570 and 1643 cm^{-1} are observed. The 1643 cm^{-1} band in the neutral benzamidine is due to the C═N stretching vibration coupled with NH_2 scissoring while the 1570 cm^{-1} band is due to the ring stretching 8b mode coupled with C═N stretching. Together, the marker bands of amidines at their protonated and neutral states allow us to define the protonation state of the amidine group for compounds I−V in the active site of UK.

Protonation State of the Ligands Bound to UK. High quality Raman spectra of compounds I−V bound separately to UK could be obtained from individual crystals in hanging drops. Figure 2 compares the Raman difference spectra of compounds I−V bound to UK crystals. Although of higher quality (discussed below), the Raman spectra from the crystal complexes are similar to the Raman difference spectra of the UK complexes in solution. The spectra in Figure 2 are dominated by contributions from the bound ligands, since the ligands are strong Raman scatterers. Contributions from the protein, resulting from a conformational change in ligand binding and protein features not subtracting to zero in the Raman difference experiment, are very weak or absent in Figure 2.

The Raman difference spectra for the five bound ligands seen in Figure 2 have the same general appearance—resulting from the dominant contributions of the common naphthyl ring to the Raman profiles. The exception is Figure 2C, for

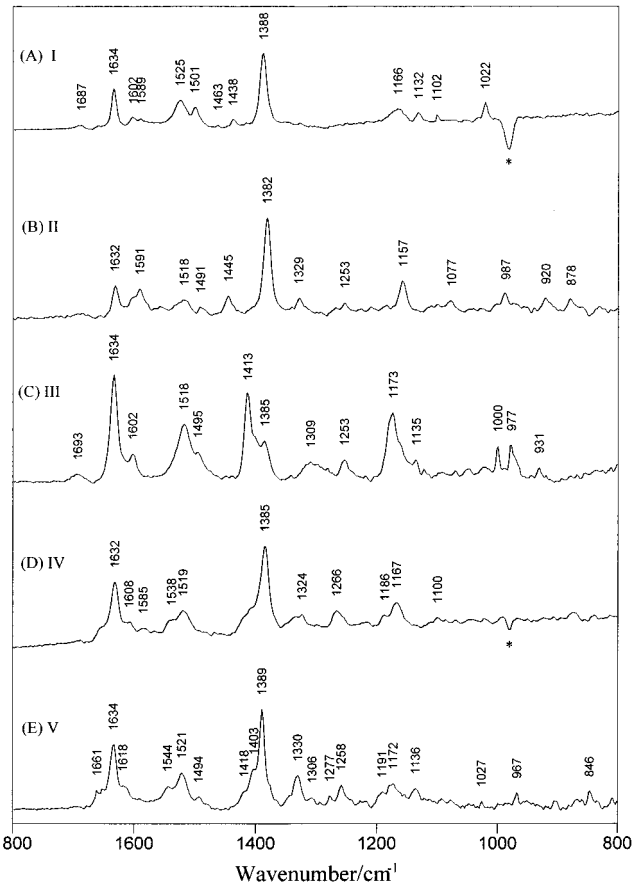

FIGURE 2: Raman difference spectra of five naphthamidine inhibitors (compounds I−V) bound to UK crystal at pH 4.7, with structures corresponding to Scheme 1. The negative bands at 980 cm^{-1} marked with asterisks in spectra A and D are due to sulfate ion. Typical conditions for data collection: 50 mW, 647.1 nm, 5 min data acquisition, 50× objective. See Experimental Procedures for spectral subtraction protocols.

compound III, where likely coupling between the naphthyl vibration near 1380 cm^{-1} and the ureido group (−NH−CO−NH−) changes the appearance of the spectral region near 1400 cm^{-1}. The other features in common are the medium intensity profiles near 1520 cm^{-1} and the weak bands near 1690 cm^{-1}. These are assigned to the amidinium group and immediately confirm that this group is protonated. This is not unexpected since the structures of the ligand−UK complexes derived by X-ray crystallographic analyses show that a salt bridge exists between the amidine group and the side chain of Asp189 (*16*, *22*−*24*). However, to the best of our knowledge, this is the first direct experimental evidence that the two groups are interacting as their charged forms, i.e., that the proton has remained on the amidine group. In a low dielectric environment, the two groups may interact as neutral species (*25*−*29*), but again the crystallographic data for the environment around the Asp189−amidinium bridge show the presence of some water molecules and thus the local dielectric cannot be uniformly low. In addition to Raman bands emanating from the naphthyl ring or the amidinium group, the spectra in Figure 2 contain contributions from other functionalities. For example, in Figure 2B,D, the pyrimidine ring contributes near 1590 cm^{-1}, and in Figure 2D,E, the peptide bond linking the aromatic rings shows weak amide I and III features near 1660 and 1260 cm^{-1},

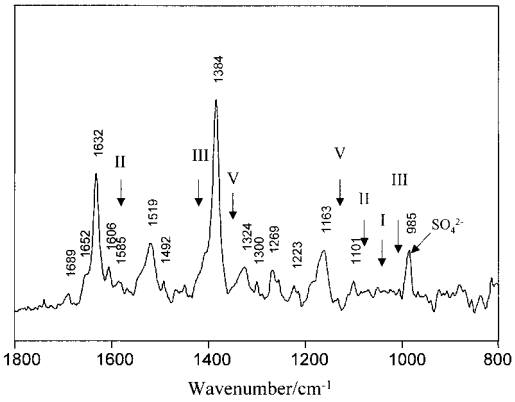

FIGURE 3: Results of a competitive inhibition experiment. Raman difference spectrum of inhibitor(s) bound to UK crystal, derived from soaking in a mixture of five inhibitors.

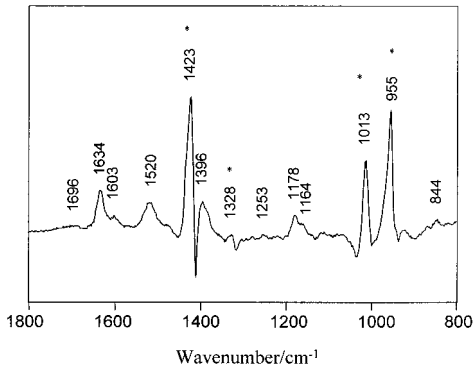

FIGURE 4: Raman spectrum of compound III (Scheme 1) bound to UK protein in solution (170 μM, buffered with 50 mM Tris-HCl at pH 7.5). 800 mW, 752 nm laser, 5 min data acquisition, 90° excitation−collection geometry. The bands denoted with asterisks are due to DMSO.

respectively. These are a source of further information on ligand−active site binding, but are not germane to the main arguments being developed here.

Competitive Binding Studies in Single Crystals. The use of crystals also allows us to extract the most potent ligand from a panel of compounds without resorting to chromatographic separation procedures, which would be required, for example, in a solution Raman study. In the competitive binding experiments, the Raman spectrum was recorded from a single crystal in a hanging drop. Subsequently, equimolar amounts of all five ligands, I−V, were added to the drop to reach a final level of 1 mM for each. The crystals were allowed to equilibrate for 24 h and transferred into a fresh hanging drop of mother liquor, before recording the spectrum of the crystal containing bound inhibitors. This step reduced the DMSO present to a negligible level. The resulting Raman difference spectrum, [UK + inhibitors] − [UK], is shown in Figure 3. The spectrum in Figure 3 is essentially identical to that for compound IV alone binding to UK and seen in Figure 2D. The following features, identified by Roman numerals in Figure 3, characteristic of compounds I−III and V, cannot be identified in Figure 3: compound I at 1022 cm^{-1}, compound II at 1591 and 1079 cm^{-1}, compound III at 1413 and 1000 cm^{-1}, compound V at 1330 and 1136 cm^{-1}. This identifies compound IV as having the greatest affinity for the active site of UK in crystals at pH 4.7, a finding consonant with the K_i values measured in the homogeneous spectrophotometric assay in pH 7.4 solution (*16*, *17*) and listed in Scheme 1. Compound IV has the lowest K_i, 0.7 nM, with compound II showing the next higher affinity at $K_i = 30$ nM. The data in Figure 3 cannot preclude small (a few percent) amounts of the other inhibitors being present, but clearly we are able to identify the most potent inhibitor.

It should be emphasized that our system has not been selected to present a "most favorable case". Rather it is the opposite: the five ligands examined have strong chemical similarities and generally similar Raman signatures. However, there remain a sufficient number of unique spectral characteristics to allow us to distinguish the bound ligand.

Comparison of Raman Data for Complexes of UK in Single Crystals and in Solution. Single crystal studies offer several advantages for obtaining Raman data of bound ligands. The concentration of active sites in the crystal is maximal and could not be matched in solution. Strong interference from bands due to the organic solvent used to carry an insoluble ligand into solution can be problematic. This is seen for compound III bound to UK in solution (Figure 4), where DMSO peaks, marked by asterisks, could not be successfully subtracted away. In contrast, the spectrum of compound III in the single crystal (Figure 2C) is free from solvent peaks. This results from the higher protein/solvent ratio found in the crystal experiments. Furthermore, removal of solvent signals in the crystal can be carried out simply by transferring the crystal complexes into a new hanging drop of mother liquor, as described under Experimental Procedures. It is worth noting that problems arising from subtracting away organic solvent bands could be minimized by using a solvent that has no bands or weak features, in the spectral region of interest. For example, deuterated DMSO has no features above 1070 cm^{-1}.

Other problems that occur in solution studies of protein−ligand complexes stem from interference from the spectral background. At low concentrations, the Raman spectrum of water itself (which is weak but finite throughout the fingerprint region) and its attendant shot-noise reduces the signal-to-noise ratio of the solute. The spectral background can also be high due to the presence of solute aggregates causing intense Rayleigh scattering, the tail of which "bleeds" into the Raman region. Both these problems are minimized in single crystal studies, and much higher quality Raman data are usually obtained from crystal, compared to solution, conditions.

The Raman crystal method could serve as a valuable routine diagnostic to assess the integrity of cocrystals, formed by either soaking or cocrystallization. Since high resolution X-ray structural data are not always readily available, Raman crystal screening may be able to rapidly infer/confirm whether the candidate compound is bound in an expected form.

A disadvantage of crystal-based experiments is the absolute requirement to grow crystals, preferably, with 20−30 μm in their minimum dimension; however, there is no strict requirement for either diffraction quality or geometry of the crystals. In addition, the experiments described here require access for the ligand to the active site in the crystal. If the active site is obscured, by molecule−molecule contacts, or if the ligand is too large, binding to the active site will not occur.

ACKNOWLEDGMENT

We thank the Ohio Supercomputer Center (Project PDS 0183) for part of the calculation work carried out on the T90 vector processor.

SUPPORTING INFORMATION AVAILABLE

Raman spectra of compounds I−V listed in Scheme 1 at solid state. This material is available free of charge via the Internet at http://pubs.acs.org.

REFERENCES

1. Altose, M. D., Zheng, Y., Dong, J., Palfey, B., and Carey, P. R. (2001) *Proc. Natl. Acad. Sci. U.S.A. 98*, 3006−3011.
2. Quax, P. H., van Leeuwen, R. T., Verspaget, H. W., and Verheijen, J. H. (1990) *Cancer Res. 50*, 1488−1494.
3. Behrendt, N., Ronne, E., Ploug, M., Petri, T., Lober, D., Nielsen, L. S., Schleuning, W. D., Blasi, F., Appella, E., and Dano, K. (1990) *J. Biol. Chem. 265*, 6453−6460.
4. Duffy, M. J. (1990) *Blood Coagulation Fibrinolysis 1*, 681−687.
5. Schmitt, M., Janicke, F., Moniwa, N., Chucholowski, N., Pache, L., and Graeff, H. (1992) *Biol. Chem. Hoppe-Seyler 373*, 611−622.
6. Magdolen, V., de Prada, A. N., Sperl, S., Muehlenweg, B., Luther, T., Wilhelm, O. G., Magdolen, U., Graeff, H., Reuning, U., and Schmitt, M. (2000) *Adv. Exp. Med. Biol. 477*, 331−341.
7. Rabbani, S., Harakidas, P., Davidson, D., Henkin, J., and Mazar, A. (1995) *Int. J. Cancer 63*, 840−845.
8. Astedt, B., Billstrom, A., and Lecander, I. (1995) *Fibrinolysis 9*, 175−177.
9. Kobayahsi, H., Gotoh, J., Shinohara, H., Moniwa, N., and Terao, T. (1994) *Thromb. Haemostasis 71*, 474−480.
10. Alonso, D., Farias, E., Ladeda, V., Davel, L., Puricelli, L., and Joffe, E. (1996) *Breast Cancer Res. Treat. 40*, 209−223.
11. Jankun, J., Keck, R., Skrzypczak-Jankun, E., and Swiercz, R. (1997) *Cancer Res. 57*, 559−563.
12. Evans, D., Sloan-Stakleff, K., Arvan, M., and Guyton, D. (1998) *Clin. Exp. Metastasis 16*, 353−357.
13. Banerji, A., Fernandes, A., Bane, S., and Ahire, S. (1998) *Cancer Lett. 129*, 15−20.
14. Alonso, D., Tejera, A., Farias, E., Joffe, E., and Bomez, D. (1998) *Anticancer Res. 18*, 4499−4504.
15. Xiao, G., Liu, Y., Gentz, R., Sang, Q., Goldberg, I., and Shi, Y. (1999) *Proc. Natl. Acad. Sci. U.S.A. 96*, 3700−3705.
16. Nienaber, V., Wang, J., Davidson, D., and Henkin, J. (2000) *J. Biol. Chem. 275*, 7237−7248.
17. Nienaber, V. L., Richardson, P. L., Klighofer, V., Bouska, J. J., Giranda, V. L., and Greer, J. (2000) *Nat. Biotechnol. 18*, 1105−1108.
18. Dong, J., Dinakarpandian, D., and Carey, P. R. (1998) *Appl. Spectrosc. 52*, 1117−1122.
19. Frisch, M. J., et al. (1998) *Gaussian 98* (Revision A.6), Gaussian, Inc., Pittsburgh, PA.
20. Scott, A. P., and Radom, L. (1996) *J. Phys. Chem. 100*, 16502.
21. Martin, J. M. L., El-Yazal, J., and Francois, J. P. (1996) *J. Phys. Chem. 100*, 15358−15367.
22. Nienaber, V. L., Davidson, D., Edalji, R., Giranda, V. L., Klinghofer, V., Henkin, J., Magdalinos, P., Mantei, R., Merrick, S., Severin, J. M., Smith, R. A., Stewart, K., Walter, K., Wang, J., Wendt, M., Weitzberg, M., Zhao, X., and Rockway, T. V. L. (2000) *Structure 8*, 553−563.
23. Katz, B. A., Mackman, R., Luong, C., Radika, K., Martelli, A., Spengeler, P. A., Wang, J., Chan, H., and Wong, L. (2000) *Chem. Biol. 7*, 299−312.
24. Zeslawska, E., Schweinitz, A., Karcher, A., Sondermann, P., Sperl, S., Sturzebecher, J., and Jacob, U. (2000) *J. Mol. Biol. 301*, 465−475.
25. Honig, B. H., and Hubbell, W. L. (1984) *Proc. Natl. Acad. Sci. U.S.A. 81*, 5412−5416.
26. Zheng, Y.-J., and Ornstein, R. L. (1996) *J. Am. Chem. Soc. 118*, 11237−11243.
27. Shimoni, L., Glusker, J. P., and Bock, C. W. (1996) *J. Phys. Chem. 100*, 2957−2967.
28. Barril, X., Aleman, C., Orozco, M., and Roque, F. J. (1998) *Proteins: Struct., Funct., Genet. 32*, 67−79.
29. Kim, Y., Lim, S., and Kim, Y. (1999) *J. Phys. Chem. A 103*, 6632−6637.

BI010955+